Applied Thermal Engineering 135 (2018) 1–9

Contents lists available at ScienceDirect

Applied Thermal Engineering

journal homepage: www.elsevier.com/locate/apthermeng

Research Paper

Heat transfer performance of flexible oscillating heat pipes for electric/hybrid-electric vehicle battery thermal management

Jian Qu[a,*], Cheng Wang[b], Xiaojun Li[a], Hai Wang[a]

[a] School of Energy and Power Engineering, Jiangsu University, Zhenjiang, Jiangsu 212013, China
[b] School of Petroleum Engineering, Changzhou University, Changzhou, Jiangsu 213016, China

HIGHLIGHTS

- Three flexible oscillating heat pipes (FOHPs) were developed.
- The FOHP performance was tested at different adiabatic lengths and structural styles.
- The "I" shape FOHPs worked well with the evaporator temperature maintained below 50 °C.
- FOHPs with small bending exhibited acceptable heat transfer performance.

ARTICLE INFO

Keywords:
Flexible oscillating heat pipe
Thermal management
Electric vehicle
Heat transfer performance
Start-up

ABSTRACT

In this paper, three flexible oscillating heat pipes (FOHPs) were experimentally tested to evaluate the effects of adiabatic length and structural style on the start-up, evaporator temperature and overall thermal resistance. The adiabatic sections of FOHPs were made of fluororubber tubes with an inner diameter of 4 mm. Deionized water was used as the working fluid at a volumetric filling ratio of 50%. The evaporator temperature could be maintained below 50 °C when the power inputs were about 121, 51 and 25 W for "I" shape FOHPs at adiabatic lengths of 570, 700 and 870 mm, respectively. The bending of adiabatic section had a negative impact on the thermo-hydrodynamic behaviour of FOHPs due to the increase in two-phase flow resistance and reduction in "pump power" provided by the gravity and therefore degrading the heat pipe performance. Although the reduction of adiabatic length reduced the evaporator temperature and elevated the FOHP performance featured by "I" and "stair-step" shapes, the best performance appeared at the adiabatic length of 700 mm for "inverted-U" and "N" shape FOHPs. FOHPs with small bending exhibited acceptable heat transfer performance, providing a possible solution for electric/hybrid-electric vehicle battery thermal management.

1. Introduction

Recent years, pure electric vehicles (EVs) and hybrid or plug-in hybrid electric vehicles (HEVs) have attracted ever-increasing attention and are considered as environment-friendly alternatives to conventional vehicles under the pressure of fossil fuel shortage and environment pollution all over the world [1,2]. As a crucial part of these low- or zero-carbon emission vehicles, lithium-ion (Li-ion) batteries with features of high power density are highly recommended as power sources to provide long driving range and fast acceleration [3]. However, Li-ion batteries generate much heat during rapid charge and discharge cycles at high current level, and thus the thermal management of them remains a big challenge as excessive local temperature rise can cause thermal runaway of individual cells or even an entire battery pack [4,5], seriously hindering the commercialization of these green energy power and clean vehicles.

To meet the operational requirements of battery thermal energy management, different cooling schemes, such as air [6], liquid (water/oil/refrigerant) [7,8], phase change material (PCM) [9,10], heat pipe [3,11–14], or a combination of them [15,16] have been proposed in the last decade. Among all of above possible cooling solutions, the hear pipe technology is a feasible approach to remove high heat dissipation densities in EV battery pack and becomes increasingly popular because of its advantages over extrusion heat sinks and pumped liquid cooling. Based on the flexible geometry that can fit variable cooling areas, heat pipes between two neighbouring batteries can remove much more heat to ambient air so that batteries can be maintained in the desired operating temperature range under variable working conditions and

* Corresponding author.
E-mail address: rjqu@ujs.edu.cn (J. Qu).

https://doi.org/10.1016/j.applthermaleng.2018.02.045
Received 3 December 2017; Received in revised form 7 January 2018; Accepted 13 February 2018
Available online 14 February 2018
1359-4311/

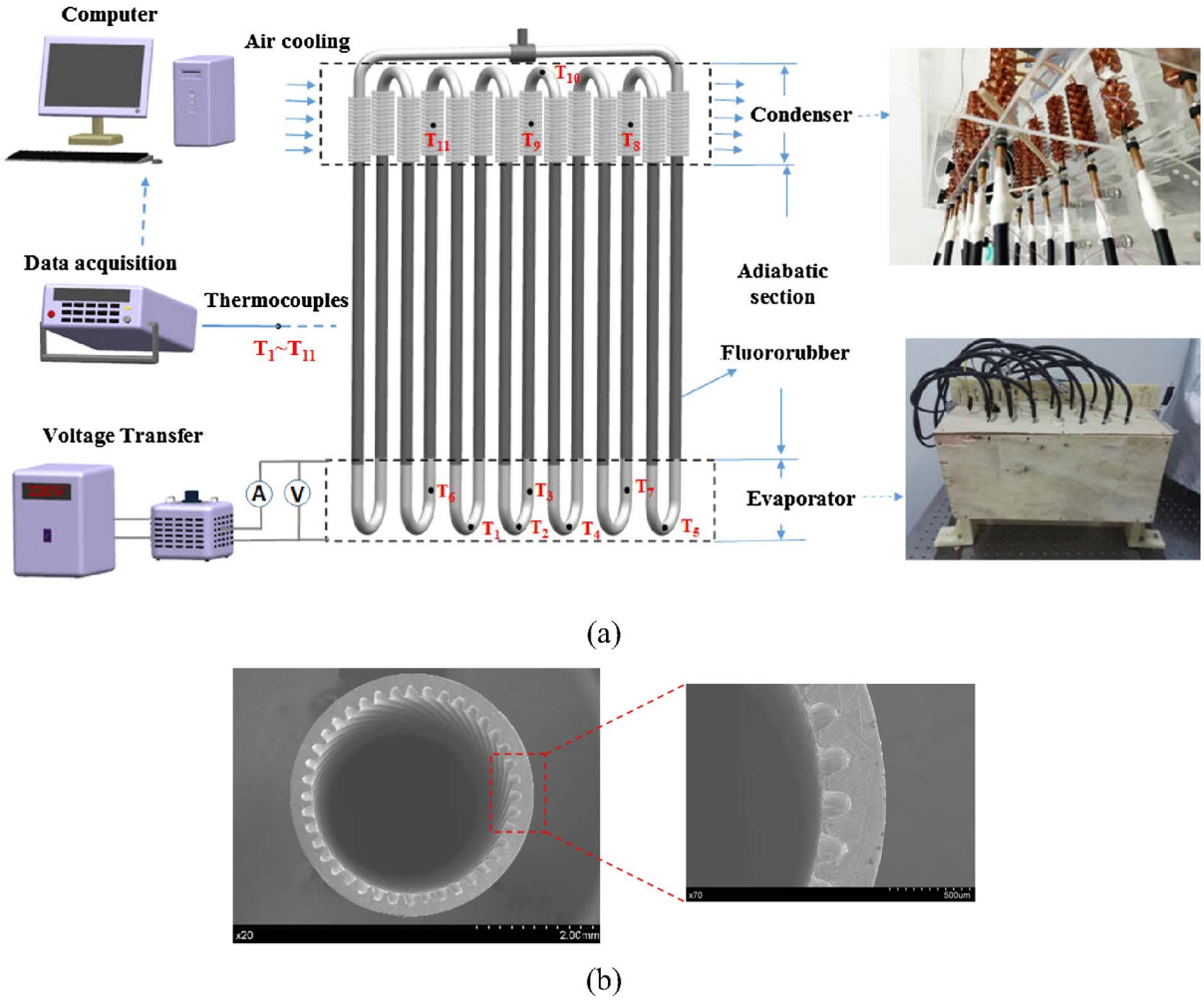

Fig. 1. Schematic diagram of the experimental setup (a) and the magnified cross-sectional image of micro-grooved copper tube (b).

therefore reducing the temperature difference between batteries significantly [12]. However, previous studies were mainly concentrated on the heat transfer performance of a single heat pipe unit or a bundle of heat pipes with wicking structures inside [12,14]. Differing from conventional heat pipes, a novel wickless and compact heat pipe, namely oscillating or pulsating heat pipe (OHP or PHP), has been proposed and considered as a promising solution in a broad range of industrial and commercial areas owning to the simplicity, high performance and versatility [17]. Actually, the serpentine-shape loop with multiple turns makes an OHP work like an array of single heat pipes, but also transfer considerable amount of sensible heat via its unique 'self-excited' thermally-driven oscillating and circulating motions of slugs/bubbles inside, and can alter its heat transfer capacity just by adjusting the turn numbers, which is highly appreciable in HEV/EV applications. To enable cost-effectiveness, compactness, lightweight, and convenient maintenance, OHPs were recently suggested [16,18,19] to use as high-efficiency heat transfer devices in EV battery cooling. Burban et al. [18] performed an experimental study to investigate the cooling performance of an open loop PHP (2.5 mm inner diameter) with an air heat exchanger to electronic devices in HEVs. Steady state and transient performance with a hybrid driving cycle (New European Driving Cycle) was conducted by altering the working fluid, inclination, air velocity and temperature. Rao et al. [19] designed and experimentally investigated an OHP-cooled battery thermal management system, and found that the maximum temperature of battery could be maintained below 50 °C when the heat generation was lower than 50 W. Most recently, Rao's group [16] tested the combined performance of PCM/OHP-based battery thermal management system; temperature variations under different heating powers, battery surrogate terminal direction and OHP placement were investigated. Experimental results demonstrated that the PCM/OHP-based system was capable of cooling power battery system more efficiently than the single OHP-based system. At the condenser regions of these OHPs, the schemes of air cooling [18] and water cooling [16,19] were utilized.

In the past two decades, most of OHPs have been constructed using rigid materials such as copper, stainless steel and silicon [20–25] due to their benefits of easy fabrication, high thermal conductivity, and good workability, while sometimes they are not compatible with the requirement of considerable heat-transport distance in space complex areas. Recently, polymers have been considered as a possible candidate material to develop flexible heat pipes due to their major advantages of flexibility, lightweight, chemical resistance and electrical insulating characteristics [26]. In 2001, McDaniels and Peterson [27] developed a flexible polymer heat pipe with grooved wicking structures and achieved a high thermal conductivity of about 740 W/(m·K). Later, advances in some other polymer heat pipes, such as flat heat pipe [28–30], cylindrical heat pipe [31], and loop heat pipe [32], were also made to become flexible two-phase spreaders. Additionally, Lin et al. [33] fabricated and tested a conceptual OHP largely made of polydimethylsiloxane (PDMS) with the length, width, and inner diameter of 56, 50 and 2 mm, respectively, in 2009. During the fabrication process, two copper blocks were used as the evaporator and condenser. The experimental results indicated that this PDMS OHP had better thermal performance when charged with methanol as compared with that of

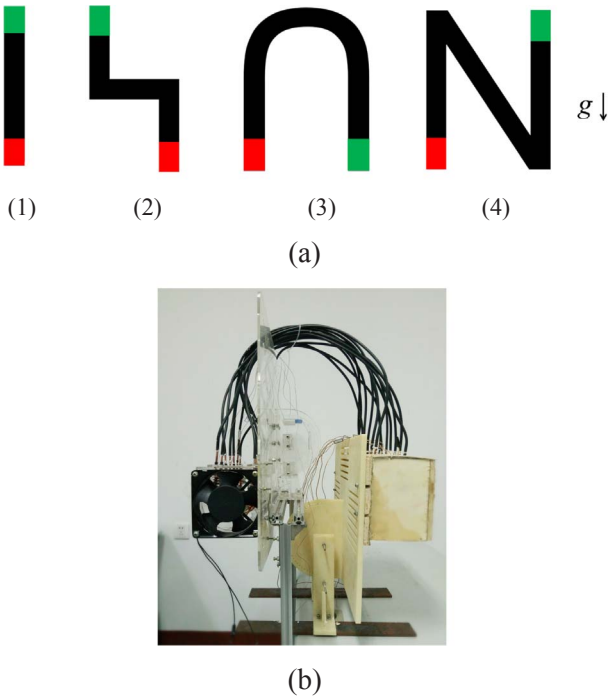

Fig. 2. Schematic diagram (a) and photograph (b) of the FOHP with four different structural styles: (1) “I” shape, (2) “stair-step” shape, (3) “inverted-U” shape, and (4) “N” shape.

ethanol. However, the thermal resistances of the OHP were relatively large, normally greater than 4.5 K/W. A similar PDMS OHP was fabricated and experimental tested by Ji et al. [34] using ethanol and Al_2O_3/ethanol nanofluid as the working fluids. Ogata et al. [35] developed a 0.34 mm-thick polymer OHP though forming with UV curable polymer resin on polyethylene terephthalate films. When electronic liquid HFE-7000 was used as the working fluid, the thermal resistance of OHP reached a minimum value at a heat load of 4.11 W, which was comparable with that of a metal plate with the same thickness. Most recently, a large-scale flexible OHP (FOHP) was designed and fabricated by Qu et al. [36]. Experimental tests showed that this FOHP could function well and exhibited highly spatial flexibility, indicating the operational feasibility of a polymer OHP at a large version on the thermal management of HEV/EV battery. As a major part of the FOHP, its adiabatic section was made of fluororubber materials due to the advantages of better heat resistance, wide range of working temperature, good shockproof capability, lower gas permeability, and excellent bendability [37]. Clearly, the adiabatic length of an FOHP directly affects its internal thermo-hydrodynamic behaviour and overall thermal performance because of the dependent effective length of heat pipe [17], especially at the spatial deformation conditions.

In this study, FOHPs with different adiabatic lengths have been experimentally studied and compared to investigate the influences of adiabatic length and structural bending on the heat transfer performance. Experimentally results indicate the usability of FOHPs to provide potential applications in HEV/EV battery thermal management involving spatial complicated structures.

2. Experimental

2.1. Experimental setup

As illustrated in Fig. 1(a), similar to the test apparatus of our earlier work [36], the experimental system mainly consists of an FOHP assembly, an electrical heating unit, a wind cooling unit, and a data measurement and acquisition system. The tube is folded in a single loop

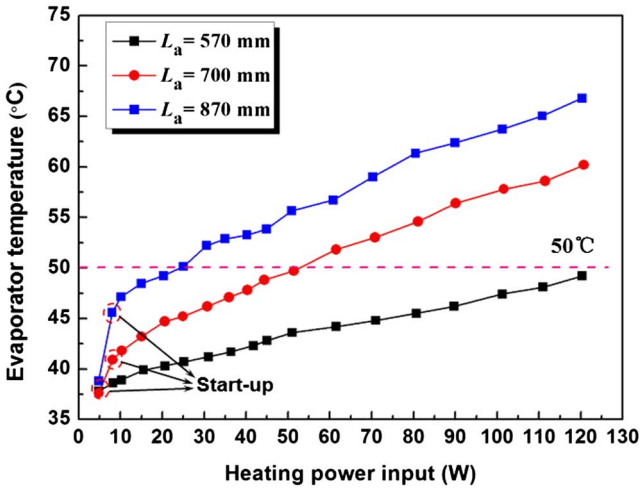

Fig. 3. Average evaporator temperature vs. heating power input for “I” shape FOHPs with different adiabatic lengths.

with seven turns at the evaporator, which is arranged in a staggered configuration. The adiabatic section of FOHP is made of fluororubber materials with inner and outer tube diameters of 4 and 6 mm, respectively. Both of the heating and cooling sections are fabricated by micro-grooved copper tubes (4 mm outer diameter as shown in Fig. 1(b)) because of their high performance as OHP materials [38,39], which is characterized by an internal equivalent diameter of about 2.0 mm. Note that the evaporator and condenser lengths are kept at 80 and 120 mm, respectively, and three adiabatic lengths, 570, 700, and 870 mm, are utilized for the performance comparison.

The heat input of FOHPs is imposed by an electric heating system, which mainly includes an AC regulated power supply, a voltage regulator, two digital multimeters and a nichrome heating wire (0.3 mm in diameter). The nichrome wire is connected in parallel and tightly wrapped around the evaporator turns. During the experiment, the evaporator was electrically heated by the heating wire and the power input was adjusted by the voltage regulator. The evaporator was well thermally insulated by aluminum foil enveloped silicate fiberglass insulation and then encased in a wooden box to minimize the heat loss from this section to the ambience. At the condenser region, it was cooled by air forced convection driven by two coaxial fans (one is a blow fan and another is a suction fan) at an ambient temperature of 25 ± 1 °C. To enhance the heat dissipation of condenser, copper fins were used on the outside of tubes.

As depicted in Fig. 1(a), eleven OMEGA K-type thermocouples are used to measure the wall temperatures of the heat pipe, which are located at different regions along the heat pipe tube and marked by points T_1-T_7 on the evaporator, and points T_8-T_{11} on the condenser. All temperature signals were collected by the data acquisition instrument (34970A, Agilent) and transferred to a computer.

Four typical structural styles were designed for these FOHPs, namely “I” shape, “stair-step” shape, “inverted-U” shape, and “N” shape, as illustrated in Fig. 2 (a). It is noted that these parts coloured by red, black, and green represent the evaporator, adiabatic and condenser sections, respectively. For example, the image of “inverted-U” shape is presented in Fig. 2(b) with structural similarity as described in Fig. 2(a-3).

The airproof test was conducted and results did not show the distinct difference between fluororubber materials and conventional rigid materials. After evacuating to a pressure below 1.0 Pa, the deformation of fluororubber tube was negligible. Degassed deionized (DI) water was used as the working fluid with a volumetric filling ratio of 50%. All of these OHPs worked at the vertical bottom-heating mode. During the experiment, the heating power input was stepwise increased until the quasi-steady state was established.

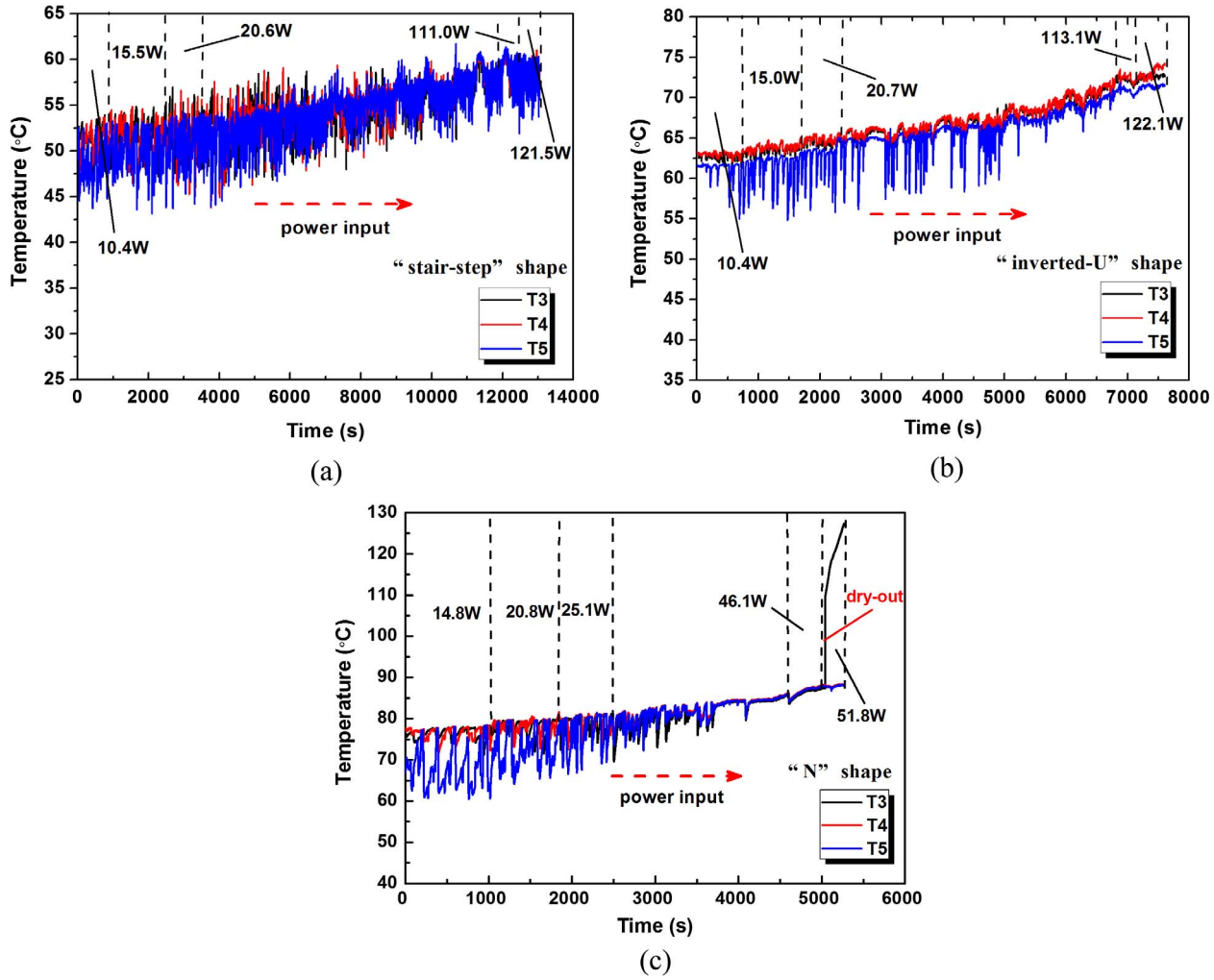

Fig. 4. Evaporator temperature variations with the power input at an adiabatic length of 570 mm for FOHPs with (a) “stair-step” shape, (b) “inverted-U” shape and (c) “N” shape.

2.2. Data reduction and uncertainty analysis

The overall thermal resistance, an important parameter indicating the heat transfer performance of an OHP, is defined as

$$R = (T_e - T_c)/Q_a \tag{1}$$

where T_e and T_c are the average wall temperatures of the evaporator and condenser, respectively, which are determined by

$$T_e = \frac{1}{7}\sum_{i=1}^{7} T_i \tag{2}$$

$$T_c = \frac{1}{4}\sum_{i=8}^{11} T_i \tag{3}$$

where T_i (i = 1, 2, …, 11) are wall temperatures measured by thermocouples allocated on the OHP as illustrated in Fig. 1(a).

Q_a in Eq. (1) is the heat input added to the evaporator. Because the evaporator of FOHP is extremely well thermally insulated, the heat loss from this section is quite small and can be approximately neglected. Therefore, the heating power input could be approximately calculated by

$$Q_a = UI \tag{4}$$

where U and I are the input voltage, electric current, respectively. In terms of Eqs. (1) and (4) as well as the error propagation principle, the uncertainties of indirect measurement parameters Q_a and R can be expressed as

$$\frac{\Delta Q_a}{Q_a} = \sqrt{\left(\frac{\Delta I}{I}\right)^2 + \left(\frac{\Delta U}{U}\right)^2} \tag{5}$$

$$\frac{\Delta R}{R} = \sqrt{\frac{(\Delta T_e)^2 + (\Delta T_c)^2}{(T_e - T_c)^2} + \left(\frac{\Delta Q_a}{Q_a}\right)^2} \tag{6}$$

The accuracies of digital multimeter to measure voltage and current were ± 0.8% and ± 1.0%, respectively. The uncertainties of direct measurement parameters, such as T_i (i = 1, 2, 3, …, 11), U and I, were synthesized by the system uncertainty from the precision of instruments and random uncertainty from the data repeatability. The maximum relative heat loss from the evaporator and adiabatic sections to the ambience is less than 4.5%. If a minimum temperature difference between the hot and cold regions is assumed to be 20 °C, the maximum uncertainty of the thermal resistance is 6.4%.

3. Results and discussion

3.1. Comparison of the evaporator temperature

Compared with structural styles having notable bending as illustrated in Fig. 2(a), the FOHP with “I” shape is actually characterized by negligible deformation and thus could work approximately like a vertical-oriented rigid OHP and has better performance [36], which is also confirmed in the present study with different adiabatic lengths.

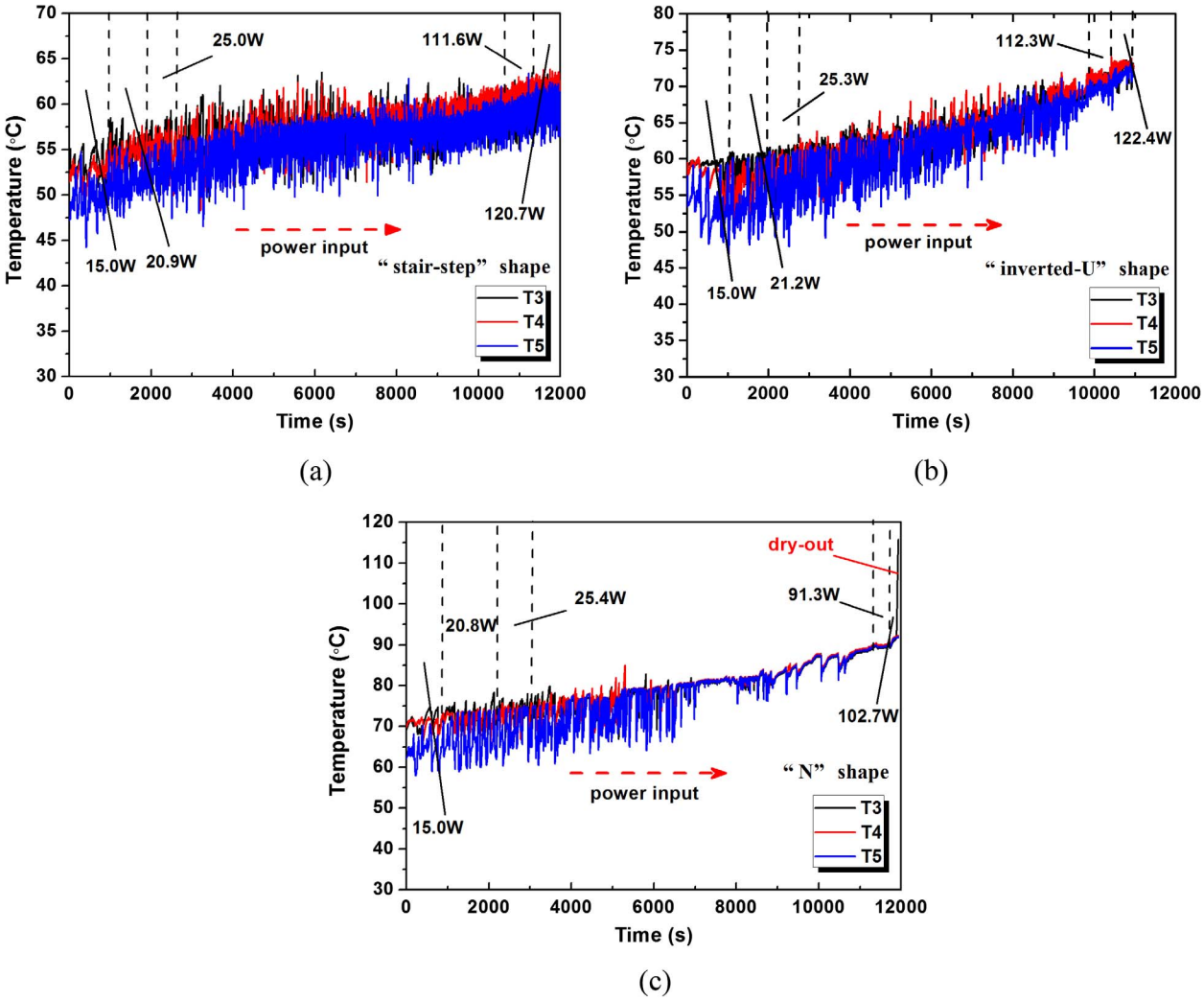

Fig. 5. Evaporator temperature variations with the power input at an adiabatic length of 700 mm for FOHPs with (a) “stair-step” shape, (b) “inverted-U” shape and (c) “N” shape.

Fig. 3 shows the average evaporator temperature versus power input of “I” shape FOHPs at different adiabatic lengths. To satisfy the safety temperature (less than 50 °C) of EV batteries and extend the cycle life [40], the maximum power input is limited to about 121 W in terms of the lowest evaporator temperature observed on these FOHPs as appeared in the adiabatic length of 570 mm. For the adiabatic lengths of 700 and 870 mm, the corresponding maximum power inputs are about 51 and 25 W, respectively, to achieve average evaporator temperature below 50 °C. As for other structural styles, higher evaporator temperatures, however, were observed under the same power input range.

Figs. 4–6 compare the evaporator temperature variations of FOHPs at quasi-steady oscillating state with different structural styles of “stair-step”, “inverted-U” and “N” shapes at adiabatic lengths of 570, 700 and 870 mm, respectively. Three typical temperature points (T_3, T_4, and T_5) were adopted below the power input of about 121 W. Obviously, the impact of adiabatic length largely depends on the FOHP structure itself. At a specific adiabatic length such as L_a = 570 mm in Fig. 4, the evaporator temperatures varied from low to high follow such an order, i.e., “stair-step” shape, “inverted-U” shape, and “N” shape. As compared to the “I” shape, the spatial deformation of adiabatic section (not involve diameter) with respect to different structural styles would definitely increase the two-phase flow resistance and engender an extra pressure loss along the tube, resulting in a negative influence on the thermo-hydrodynamic behaviour inside the FOHP. In addition, the bending of adiabatic section can change the gravity effect on the OHP greatly. Usually, the gravity acts as a positive driving force and provides the“pump power” to facilitate the backflow of condensate towards the evaporator in a vertical-oriented OHP, which supplies the liquid to maintain continuous boiling and evaporation in the hot region [22]. Gravity renders the interval unbalanced pressure oscillation inside the OHP as well, enabling the whole slug-plug system to overcome the pressure dissipation and support the oscillatory mass and heat transport between the evaporator and condenser [41,42]. However, the fluid movement in the adiabatic section is partially under the horizontal (see Fig. 2(a2)) or even anti-gravity (see Fig. 2(a3) and (a4)) condition due to the structural deformation, significantly degrading the robust oscillation and yielding much higher evaporator temperatures.

In addition, the start-up evaporator temperatures were also increased significantly due to the deformation of adiabatic section. The average start-up evaporator temperatures of FOHPs featured by different structural styles are summarized in Table 1. For example, the start-up temperatures are 37.8, 52.7, 63.5 and 75.4 °C for FOHPs featured by “I” shape, “stair-step” shape, “inverted-U” shape and “N” shape, respectively, when the adiabatic length is 570 mm. Similar results were obtained for other two adiabatic lengths of 700 and 870 mm. Generally, the start-up of an OHP always stem from heat input induced local bubble generation and expansion at the evaporator section, suddenly triggering the overall oscillating motions of slugs/plugs inside. At the same filling ratio, the structural style of adiabatic region may not significantly affect the local bubble nucleation at the evaporator region under the same heat input, while the structural deformation and induced spatial arrangement of evaporator and condenser can profoundly

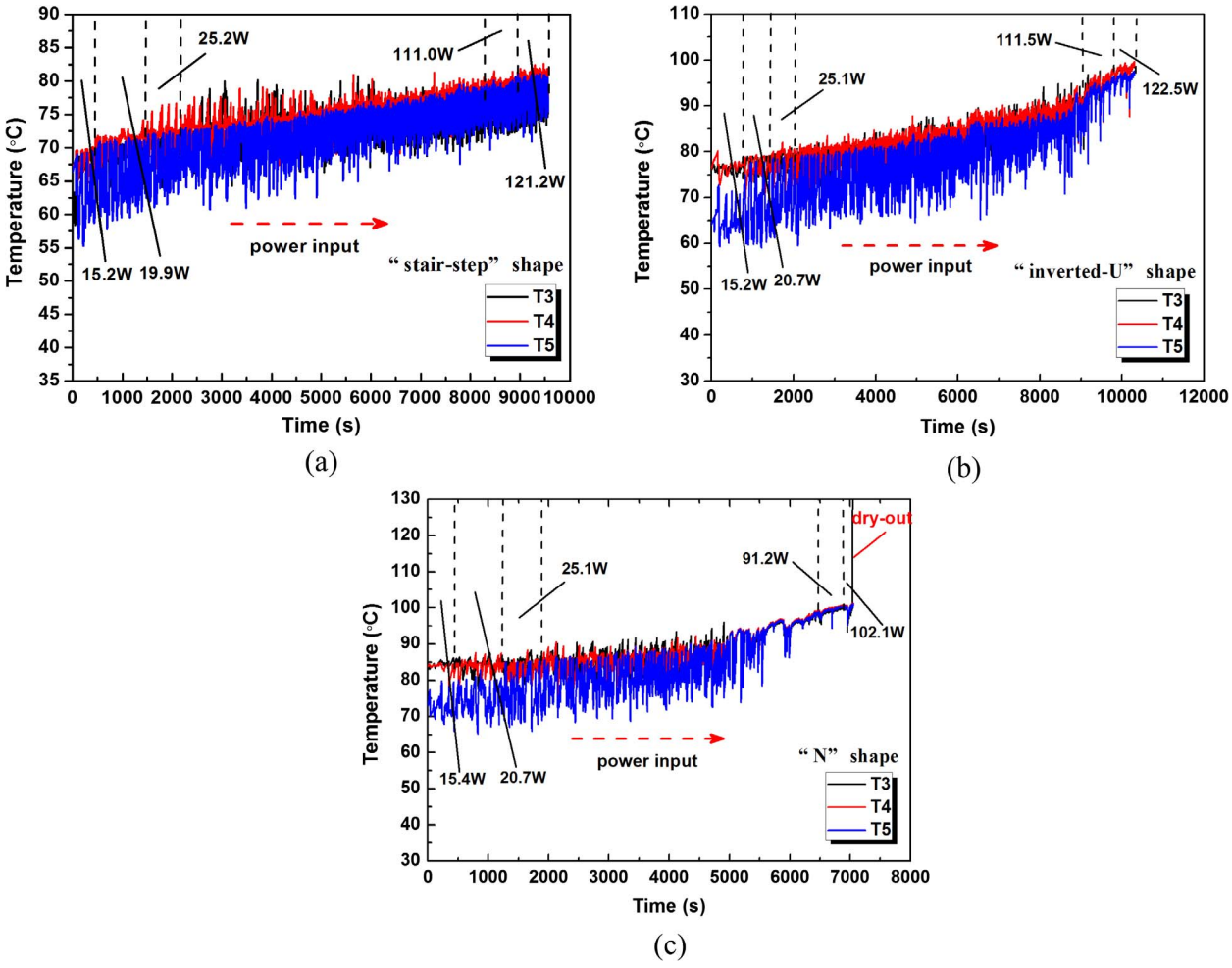

Fig. 6. Evaporator temperature variations with the power input at an adiabatic length of 870 mm for FOHPs with (a) “stair-step” shape, (b) “inverted-U” shape and (c) “N” shape.

Table 1
Start-up evaporator temperatures of FOHPs at different adiabatic lengths.

Structural style	Start-up evaporator temperatures (°C)		
	L_a = 570 mm	L_a = 700 mm	L_a = 870 mm
“I” shape	37.8	40.9	45.6
“stair-step” shape	52.7	54.0	64.3
“inverted-U” shape	63.5	61.8	73. 6
“N” shape	75.4	72.1	81.5

enlarge the two-phase flow resistance, primarily because of the local-bending induced pressure loss. Consequently, the overall oscillating motions cannot be fully triggered and decay until a higher heat input is imposed. As for a specific structural style in Table 1, the start-up evaporator temperature largely increases with the increase of adiabatic length except for “inverted-U” and “N” shape styles. For example, the start-up evaporator temperatures of FOHPs featured by “stair-step” shape are 52.7, 54.2, and 64.3 °C at the adiabatic lengths of 570, 700, and 870 mm, respectively. Actually, the increase of adiabatic length relates to the increase in effective length as the heating and cooling lengths remain unchanged, which is disadvantage for the OHP performance [17,43]. This reason may come from that the frictional pressure drop of fluid flow reduces at a shorter effective length, and then the working fluid is vulnerable to flow from the evaporator to the condenser and vice versa, facilitating the OHP start-up and stable oscillation. However, the total pressure drop at the adiabatic section is derived from the collective effect of frictional force as well as the tube bending for each specific structural style. Even though the fluid in the FOHP (L_a = 570 mm) may encounter a lower frictional pressure drop at this section as compared to other two lengths of 700 and 870 mm, the reduction of bend curvature radius can cause larger local pressure loss from tube bending. Hence, there exists an optimal adiabatic length with respect to the minimum total pressure loss when a strong spatial deformation, such as“inverted-U” and “N” shapes, is used, and L_a = 700 mm seems to be the appropriate value according to Figs. 4–6. By comparing the temporal variations of evaporator temperature, it can be concluded that the average evaporator temperatures become large as increasing the adiabatic length from 570 to 870 mm for “I” shape (see Fig. 3) and “stair-step” shape (see Figs. 4–6), while they decrease initially from 570 to 700 mm and then increase from 700 to 870 mm for“inverted-U” and “N” shapes.

Within the power input range less than about 121 W, the evaporator temperatures are proportional to power input for all of these OHPs at different adiabatic lengths, while the dry-out only appeared in the “N” shape style (see Figs. 4(d), 5(d) and 6(d)). The dry-out occurs at relatively lower power inputs of this structural style indicating that it has a smaller heat transport limitation as compared to other styles. Actually, the dry-out is a gradual phenomenon and some tubes initially undergo a sudden dry-out probably due to the fluid motion dampening or local dry-out, leading to a dramatic increase of corresponding evaporator temperatures and finally disorder the quasi-steady state. Note that the local dry-out in Figs. 4(d), 5(d) and 6(d) was only detected by the temperature point of T_3 owing to the less local liquid accumulation capability and consequently more dry-patch coalescence as compared to the thermocouple regions of T_4 and T_5, but the total dry-out was not

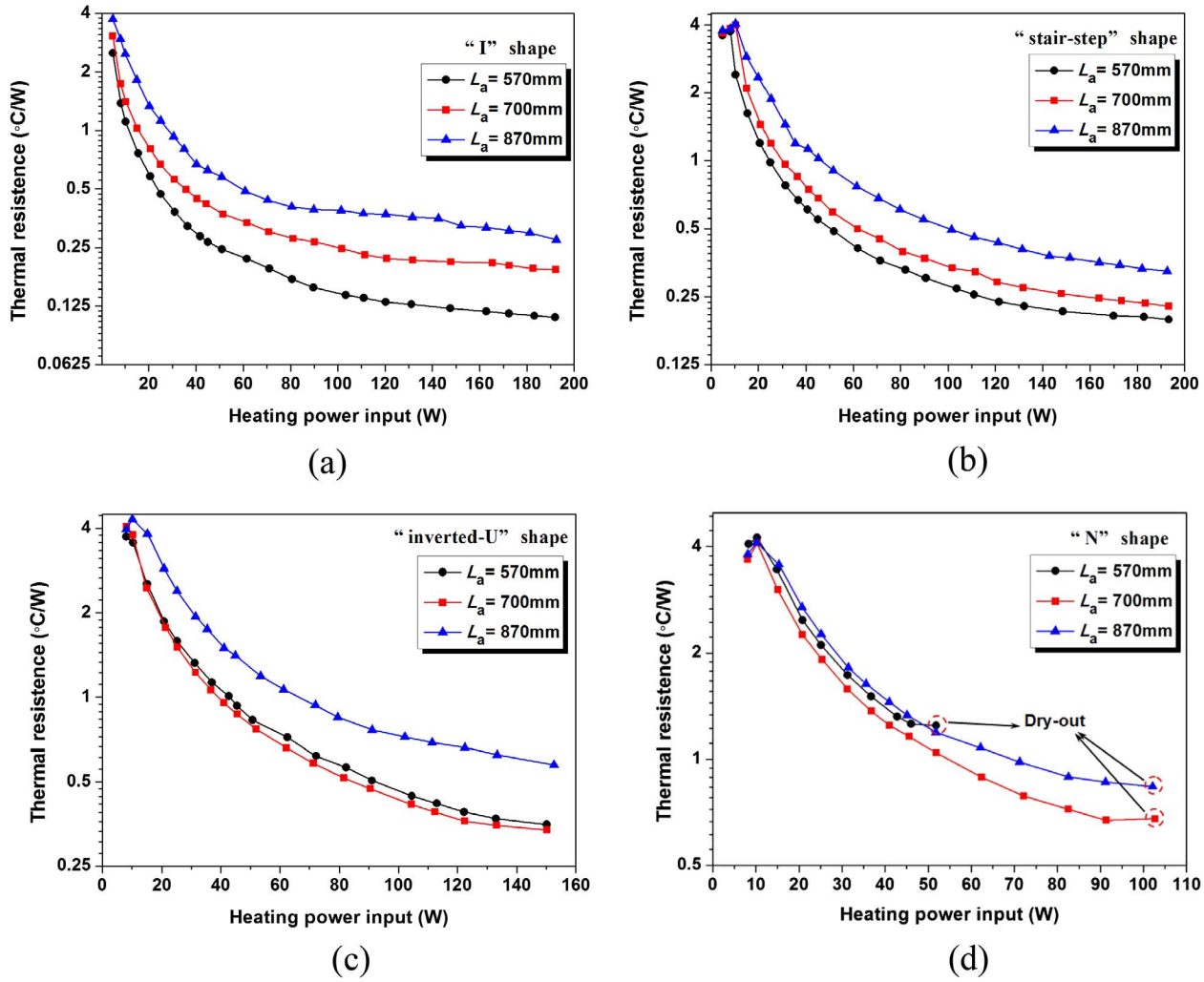

Fig. 7. Thermal resistance vs. heating power input for FOHPs featured by different structural styles.

reached. The dry-out power inputs are about 51.8, 102.7, and 102.1 W at the adiabatic lengths of 570, 700, and 870 mm, respectively. Clearly, the reduction of adiabatic length is unable to extend the dry-out power input of "N" shape FOHP and hence the adiabatic length of 570 mm refers to the minimum heat transport limitation. It can be explained that the reduction of adiabatic length truly reduces the frictional resistance, but it also causes the increase in local resistance derived from tube-bending as discussed earlier and hence overwhelmingly hinders the fluid motion, leading to the early occurrence of local dry-out eventually. Further work is needed to select proper tube diameters and working fluids to reduce the start-up temperature and operation temperature especially at large bending styles, which is desirable for the electric/hybrid-electric vehicle battery thermal management.

3.2. Comparison of the thermal resistance

Fig. 7 shows the thermal resistance variations of FOHPs at different adiabatic lengths versus heating power input. It is apparent that the structural style significantly affects the heat transfer performance. Usually, a lower thermal resistance accounts for higher heat transfer performance of an OHP, and therefore the FOHP with "I" shape has the best performance in comparison with other structural styles at each same adiabatic length. Although the heating and cooling conditions of the FOHP remain unchanged at different structural styles, the deformation of adiabatic section would inevitably enlarge the two-phase flow resistance and play a negative role in the FOHP performance. Compared to "inverted-U", "stair-step", and "N" shapes, the FOHP with "I" shape can operate similar to a vertical-oriented rigid OHP and hence encounter smaller flow resistance. Besides, the gravity distribution associated with the orientation at different parts of the OHP should also be considered. It is clear that the spatial deformation of FOHP would lower the gravity action as mentioned in Section 3.1 and then the heat transfer performance. As a result, the flexible deformation of the FOHP towards "stair-step", "inverted-U", and "N" shapes degraded the performance, and so the FOHP performance at each same adiabatic length varied from high to low in light of the structural style follows such an order, i.e., "I" shape, "stair-step" shape, "inverted-U" shape, and "N" shape.

Furthermore, the thermal resistances of both "I" and "stair-step" shape FOHPs increase as the adiabatic length becomes larger (see Fig. 7(a) and (b)), which is mainly due to the increase of frictional pressure drop and greatly restrains the oscillating motions of slugs/plugs. Under the power input of about 192 W, the thermal resistances as low as 0.11, 0.19, and 0.27 °C/W were achieved at the adiabatic lengths of 570, 700, and 870 mm, respectively. When "inverted-U" and "N" shape FOHPs were used, however, the best heat transfer performance largely appeared at the moderate adiabatic length of 700 mm as depicted in Fig. 7(c) and (d). According to aforementioned analysis, the total pressure drop in the FOHP is determined by the collective effect of frictional force and the tube bending. As for an FOHP featured by remarkable spatial deformation, the reduction of adiabatic length can significantly increase the local flow resistance induced by tube bending

and then the total pressure loss, even though the frictional pressure drop of fluid flow may be reduced. As a result, the optimal adiabatic length of 700 mm with respect to the thermal resistance is observed in the "inverted-U" shape and "N" shape FOHPs.

According to above experimental results, it can be concluded that the spatial arrangement of evaporator and condenser has a profound influence on the FOHP performance. Actually, the deformation of adiabatic section with respect to different structural styles will cause an extra pressure loss along the tube inside and greatly impact the gravity action on the FOHP, not only partially degrade the heat transfer performance, but also affect the start-up and heat transport limitation.

4. Conclusions

In the present study, three flexible OHPs with adiabatic section made of fluororubber tubes were fabricated, and microgroove copper tubes were utilized for the evaporator and condenser due to their excellent heat transport capability. The heat transfer performance of these FOHPs at different adiabatic lengths of 570, 700, and 870 mm as well as different structural styles of "I" shape, "stair-step" shape, "inverted-U" shape, and "N" shape, was experimentally studied and compared at the vertical bottom-heating mode. The experimental results demonstrated that flexible OHPs function satisfactorily especially at the "I" and "stair-step" shape styles and exhibit the usability for electric/hybrid-electric vehicle battery thermal management. The main conclusions are summarized as follows:

(1) The start-up temperatures of these FOHPs at a specific adiabatic length varied from low to high in terms of the structural style follows an order of "I" shape, "stair-step" shape, "inverted-U" shape, and "N" shape. For a specific structural style, the start-up temperature largely increased as the adiabatic length became larger.
(2) To satisfy the evaporator temperature below 50 °C, the maximum allowable heat inputs were about 121, 51 and 25 W for the "I" shape FOHPs at the adiabatic lengths of 570, 700 and 870 mm, respectively, while higher evaporator temperatures were obtained as the spatial deformation of these FOHPs towards "stair-step", "inverted-U", and "N" shapes. In addition to "I" shape FOHPs, the increase in adiabatic length also led to the increase of evaporator temperatures for "stair-step" shape FOHPs, while an optimal adiabatic length of 700 mm was observed to achieve relatively lower evaporator temperatures for "inverted-U" and "N" shapes.
(3) The heat transfer performance of these FOHPs varied from high to low according to the structural style follows an order of "I" shape, "stair-step" shape, "inverted-U" shape, and "N" shape. The thermal resistance was proportional to the adiabatic length for "I" and "stair-step" shape FOHPs within the power input of about 4.8–192 W, and a minimum thermal resistance of 0.11 °C/W was achieved for the "I" shape FOHP at the power input of 192 W. For "inverted-U" and "N" shape FOHPs, however, the lowest thermal resistance appeared at the adiabatic length of 700 mm. The dry-out only occurred in the "N" shape FOHPs and dry-out power inputs were about 51.8, 102.7, and 102.1 W at the adiabatic lengths of 570, 700, and 870 mm, respectively.

Acknowledgements

Financial grants from the National Natural Science Foundation of China (Nos. 51576091 and 51306023) are gratefully acknowledged.

References

[1] C. Mi, M.A. Masrur, Hybrid Electric Vehicles: Principles and Applications with Practical Perspectives, Wiley, 2017.
[2] M.A. Hannan, M.S.H. Lipu, A. Hussain, A. Mohamed, A review of lithium-ion battery state of charge estimation and management system in electric vehicle applications: challenges and recommendations, Renew. Sustain. Energy Rev. 78 (2017) 834–854.
[3] T.H. Tran, S. Harmand, B. Sahut, Experimental investigation on heat pipe cooling for Hybrid Electric Vehicle and Electric Vehicle lithium-ion battery, J. Power Sources 265 (2014) 262–272.
[4] Q. Wang, P. Ping, X. Zhao, G. Chu, J. Sun, C. Chen, Thermal runaway caused fire and explosion of lithium ion battery, J. Power Sources 208 (2012) 210–224.
[5] L. Lu, X. Han, J. Li, J. Hua, M. Ouyang, A review on the key issues for lithium-ion battery management in electric vehicles, J. Power Sources 226 (2013) 272–288.
[6] R. Sabbah, R. Kizilel, J.R. Selman, S. Al-Hallaj, Active (air-cooled) vs. passive (phase change material) thermal management of high power lithium-ion packs: limitation of temperature rise and uniformity of temperature distribution, J. Power Sources 182 (2008) 630–638.
[7] L.W. Jin, P.S. Lee, X.X. Kong, Y. Fan, S.K. Chou, Ultra-thin minichannel LCP for EV battery thermal management, Appl. Energy 113 (2014) 1786–1794.
[8] Y. Huo, Z. Rao, X. Liu, J. Zhao, Investigation of power battery thermal management by using mini-channel cold plate, Energy Convers. Manage. 89 (2015) 387–395.
[9] X. Duan, G.F. Naterer, Heat transfer in phase change materials for thermal management of electric vehicle battery modules, Int. J. Heat Mass Transf. 53 (2010) 5176–5182.
[10] Z. Rao, S. Wang, G. Zhang, Simulation and experiment of thermal energy management with phase change material for ageing $LiFePO_4$ power battery, Energy Convers. Manage. 52 (12) (2011) 3408–3414.
[11] J.C. Jang, S.H. Rhi, Battery thermal management system of future electric vehicles with loop thermosyphon, US-Korea Conference on Science, Technology and Entrepreneurship (UKC), 2010.
[12] Z. Rao, S. Wang, M. Wu, Z. Lin, F. Li, Experimental investigation on thermal management of electric vehicle battery with heat pipe, Energy Convers. Manage. 65 (2013) 92–97.
[13] F. Liu, F. Lan, J. Chen, Dynamic thermal characteristics of heat pipe via segmented thermal resistance model for electric vehicle battery cooling, J. Power Sources 321 (2016) 57–70.
[14] H. Zou, W. Wang, G. Zhang, F. Qin, C. Tian, Y. Yan, Experimental investigation on an integrated thermal management system with heat pipe heat exchanger for electric vehicle, Energy Convers. Manage. 118 (2016) 88–95.
[15] S. Al-Hallaj. Safety and thermal management for li-ion batteries in transportation applications, presented at the EV Li-ion Battery Forum Europe. Barcelona, Spain, 2012.
[16] Q. Wang, Z. Rao, Y. Huo, S. Wang, Thermal performance of phase change material/oscillating heat pipe-based battery thermal management system, Int. J. Therm. Sci. 102 (2016) 9–16.
[17] J. Qu, Q. Wang, Experimental study on the thermal performance of vertical closed-loop oscillating heat pipes and correlation modelling, Appl. Energy 112 (2013) 1154–1160.
[18] G. Burban, V. Ayel, A. Alexandre, P. Lagonotte, Y. Bertin, C. Romestant, Experimental investigation of a pulsating heat pipe for hybrid vehicle applications, Appl. Therm. Eng. 50 (1) (2013) 94–103.
[19] Z. Rao, Y. Huo, X. Liu, Experimental study of an OHP-cooled thermal management system for electric vehicle power battery, Exp. Therm. Fluid Sci. 57 (2014) 20–26.
[20] H.B. Ma, C. Wilson, Q. Yu, K. Park, U.S. Choi, M. Tirumala, An experimental investigation of heat transport capability in a nanofluid oscillating heat pipe, J. Heat Transf. 128 (2006) 1213–1216.
[21] Q. Cai, C. Chen, J.F. Asfia, Operating characteristic investigations in pulsating heat pipe, J. Heat Transf. 128 (2006) 1329–1334.
[22] H. Yang, S. Khandekar, M. Groll, Performance characteristics of pulsating heat pipes as integral thermal spreaders, Int. J. Therm. Sci. 48 (4) (2009) 815–824.
[23] J. Qu, H. Wu, Thermal performance comparison of oscillating heat pipes with SiO_2/water and Al_2O_3/water nanofluids, Int. J. Therm. Sci. 50 (2011) 1954–1962.
[24] X. Liu, Y. Chen, M. Shi, Dynamic performance analysis on start-up of closed-loop pulsating heat pipes (CLPHPs), Int. J. Therm. Sci. 65 (2013) 224–233.
[25] Q. Sun, J. Qu, J. Yuan, Q. Wang, Operational characteristics of an MEMS-based micro oscillating heat pipe, Appl. Therm. Eng. 124 (2017) 1269–1278.
[26] J. Qu, H. Wu, P. Cheng, Q. Wang, Q. Sun, Recent advances in MEMS-based micro heat pipes, Int. J. Heat. Mass Transf. 110 (2017) 294–313.
[27] D. McDaniels, G.P. Peterson, Investigation of polymer based micro heat pipes for a flexible radiator, Publ.-HTD-ASME 369 (2001) 423–434.
[28] C. Oshman, B. Shi, C. Li, R. Yang, Y.C. Lee, G.P. Peterson, V.M. Bright, The development of polymer-based flat heat pipes, J. Microelectromech. Syst. 20 (2) (2011) 410–417.
[29] C. Oshman, Q. Li, L.A. Liew, R. Yang, V.M. Bright, Y.C. Lee, Flat flexible polymer heat pipes, J. Micromech. Microeng. 23 (2013) 015001.
[30] K.S. Yang, T.Y. Yang, C.W. Tu, C.T. Yeh, M.T. Lee, A novel flat polymer heat pipe with thermal via for cooling electronic devices, Energy Convers. Manage. 100 (2015) 37–44.
[31] C. Yang, C. Chang, C.Y. Song, W. Shang, J. Wu, P. Tao, Fabrication and performance evaluation of flexible heat pipes for potential thermal control of foldable electronics, Appl. Therm. Eng. 95 (2016) 445–453.
[32] H. Ye, R. Sokolovskij, H.W. Zeijl, A.W.J. Gielen, G. Zhang, A polymer based miniature loop heat pipe with silicon substrate and temperature sensors for high brightness light-emitting diodes, Microelectron. Reliab. 54 (2014) 1355–1362.
[33] Y. Lin, S. Kang, T. Wu, Fabrication of polydimethylsiloxane (PDMS) pulsating heat pipe, Appl. Therm. Eng. 29 (2) (2009) 573–580.
[34] Y. Ji, G. Liu, H. Ma, G. Li, Y. Sun, An experimental investigation of heat transfer performance in a polydimethylsiloxane (PDMS) oscillating heat pipe, Appl. Therm. Eng. 61 (2) (2013) 690–697.
[35] S. Ogata, E. Sukegawa, T. Kimura, Performance evaluation of ultra-thin polymer

pulsating heat pipes, in: 14th IEEE Thermal and Thermomechanical Phenomena in Electronic Systems Conference, 2014, pp. 519–526.
[36] J. Qu, X. Li, Y. Cui, Q. Wang, Design and experimental study on a hybrid flexible oscillating heat pipe, Int. J. Heat Mass Transf. 107 (2017) 640–645.
[37] M.A. Kader, A.K. Bhowmick, Thermal ageing, degradation and swelling of acrylate rubber, fluororubber and their blends containing polyfunctional acrylates, Polym. Degrade. Stabil. 79 (2003) 283–295.
[38] J. Qu, X. Li, Q. Wang, F. Liu, H. Guo, Heat transfer characteristics of micro-grooved oscillating heat pipes, Exp. Therm. Fluid Sci. 85 (2017) 75–84.
[39] J. Qu, X. Li, Q. Xu, Q. Wang, Thermal performance comparison of oscillating heat pipes with and without helical micro-grooves, Heat Mass Transf. 53 (11) (2017) 3383–3390.
[40] Q. Wang, B. Jiang, B. Li, Y. Yan, A critical review of thermal management models and solutions of lithium-ion batteries for the development of pure electric vehicles, Renew. Sustain. Energy Rev. 64 (2016) 106–128.
[41] Z. Deng, Y. Zheng, X. Liu, B. Zhu, Y. Chen, Experimental study on thermal performance of an anti-gravity pulsating heat pipe and its application on heat recovery utilization, Appl. Therm. Eng. 125 (2017) 1368–1378.
[42] J. Qu, Q. Wang, Q. Sun, Lower limit of internal diameter for oscillating heat pipes: a theoretical model, Int. J. Therm. Sci. 110 (2016) 174–185.
[43] Z. Lin, S. Wang, J. Chen, J. Huo, Y. Hu, W. Zhang, Experimental study on effective range of miniature oscillating heat pipes, Appl. Therm. Eng. 31 (2011) 880–886.